Analytical Methods

ROYAL SOCIETY OF CHEMISTRY

CRITICAL REVIEW

View Article Online
View Journal | View Issue

Cite this: *Anal. Methods*, 2024, **16**, 2810

Integrated microfluidic platforms for heavy metal sensing: a comprehensive review

Sharmila Sajankila Nadumane,[a] Rajib Biswas[b] and Nirmal Mazumder *[a]

Heavy metals are found naturally; however, anthropogenic activities such as mining, inappropriate disposal of industrial waste, and the use of pesticides and fertilizers containing heavy metals can cause their unwanted release into the environment. Conventionally, detection of heavy metals is performed using atomic absorption spectrometry, electrochemical methods and inductively coupled plasma-mass spectrometry; however, they involve expensive and sophisticated instruments and multistep sample preparation that require expertise for accurate results. In contrast, microfluidic devices involve rapid, cost-efficient, simple, and reliable approaches for in-laboratory and real-time monitoring of heavy metals. The use of inexpensive and environment friendly materials for fabrication of microfluidic devices has increased the manufacturing efficiency of the devices. Different types of techniques used in heavy metal detection include colorimetry, absorbance-based, and electrochemical detection. This review provides insight into the detection of toxic heavy metals such as mercury (Hg), cadmium (Cd), lead (Pb), and arsenic (As). Importance is given to colorimetry, optical, and electrochemical techniques applied for the detection of heavy metals using microfluidics and their modifications to improve the limit of detection (LOD).

Received 19th February 2024
Accepted 28th March 2024

DOI: 10.1039/d4ay00293h

rsc.li/methods

Introduction

Toxicity of heavy metals such as mercury (Hg), manganese (Mn), cadmium (Cd), lead (Pb), arsenic (As) and nickel (Ni), is caused due to their accumulation inside the organs of the human body. Although heavy metals naturally occur, they are also introduced into the environment through various human activities that include disposal of unprocessed industrial waste into water sources, mining, and the use of chemical-based fertilizers in agriculture (Fig. 1).[1–4] Of these heavy metals, As, Cd, Pb and Hg are recognized as the most toxic. Cd is a silvery white metal with a bluish tinge of atomic number 48 which exists as compounds with organic amines, sulphur groups, and chlorine groups. The stable isotopes of Cd are ^{106}Cd, ^{108}Cd, ^{110}Cd, ^{111}Cd, ^{112}Cd, ^{113}Cd, ^{114}Cd, and ^{116}Cd.[5] Cd enters the human body through food, water, and dust or through dermal absorption and causes cancers of the lung, breast, prostate, pancreas, urinary bladder, and nasopharynx.[5]

Pb is a bluish-grey metal that is found in the range between 10 and 30 mg kg^{-1} in the Earth's crust. Naturally Pb occurs as compounds such as PbS, $PbSO_4$, $PbCO_3$ and they exist in two ionic forms: +2 and +4. Pb gains access to the human body through the inhalation of polluted dust or through contaminated food or water.[6] Even at extremely low levels, Pb can show adverse effects in the human body, such as saturnism or plumbism that mainly affect the gastrointestinal system and nervous system.[7] With an atomic number of 33, it is the twentieth most abundant heavy metalloid found in the Earth's crust.[8] Pb is commonly found as sulfide-bearing ores.[9,10] In nature, weathering causes arsenic sulphides to convert to arsenic trioxide, which enters the arsenic cycle as dust or through dissolution in water. Excessive exposure to As affects the kidney, lungs, cardiovascular system, and respiratory system.[11] Hg is a heavy metal of the d-block of the periodic table. In nature, Hg exists in an elemental, inorganic format and possesses diverse toxicity and bioavailability.[12] Hg usually exists in Hg^{2+}, Hg^{2++}, Hg, or in the alkylated form. The intake of these mercuric forms causes Minamata disease that affects the nervous system, mainly cerebellar cortices and peripheral sensory nerves.[13] Table 1 lists the sources, effects, and permissible concentrations of various heavy metals. The amount of heavy metals on the surface and in groundwater has increased during the last few years; consequently, there is a need for regular water quality assessments.[14] Frequently used techniques for heavy metal analysis include atomic absorption spectroscopy (AAS),[15] atomic fluorescence spectroscopy,[16] and inductively coupled plasma-mass spectrometry (ICP-MS).[17]

High versatility toward simultaneous metal detection, sensitivity, specificity, accurate detection, and detection limits in the femtomolar range are a few advantages of these methods[18] (Table 2). However, they show certain drawbacks,

[a]*Department of Biophysics, Manipal School of Life Sciences, Manipal Academy of Higher Education, Manipal, Karnataka, India-576104*
[b]*Applied Optics and Photonics Laboratory, Department of Physics, Tezpur University, Tezpur, Assam, India -784028*

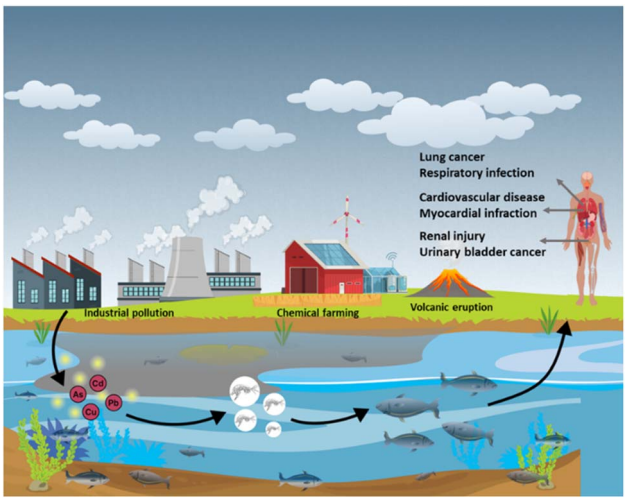

Fig. 1 Sources of heavy metals and their adverse effects on the human body.

such as requiring expensive and sophisticated instruments with the need for multistep sample preparation that requires expertise for accurate results.[19,20] As a result, the need for quick, economically beneficial, simple, and reliable approaches for in-laboratory and real-time monitoring of heavy metals has increased, prompting the advancement of sensors.[6,10,21] Lately, sensing of heavy metal ions using microfluidics has grabbed the attention of the global community. Researchers are now resorting to this fast-sensing scheme where minimal logistics can be deployed with enhanced accuracy. Accordingly, several articles on heavy metal detection using microfluidic-based devices have been published.[22–24] However, available literature caters to different adaptations of microfluidics to achieve sensing. There is a need for a comprehensive review of all these adaptations where readers can grasp the basics as well as an understanding of the potential of this growing branch of sensing. With this aim, the current review is an attempt to provide an overview of microfluidics in heavy metal detection. It will highlight the integration of techniques such as colorimetry, absorbance, fluorescence and electrochemical detection with microfluidics for detecting heavy metals. Accordingly, the following sections summarize the different routes adopted for microfluidic-based heavy metal sensing along with potentialities.

Microfluidic devices for heavy metal detection

Microfluidic devices involve the precise handling of samples in micro- or nano liters.[25] Microfluidic devices are integrated with microchannels, micropumps, and microchips that manipulate the properties of the liquid. Microfluidic systems exhibit important fluid properties, such as laminar airflow, which introduces micromachining and microoperation that cannot be incorporated into conventional techniques.[26] The experimental procedures used in the research laboratory, such as preparation of the sample, chemical reaction, separation, and detection, can be replicated in the microscale devices using a microfluidic chip, therefore referred to as a lab on a chip.[10] Compared to

Table 1 Sources, effects, and permissible limits of heavy metals in water (WHO 2017)

Heavy metals	Sources	Permissible amount (ppb)	Effect	Reference
Arsenic (As)	Mining, smelting, arsenic-containing pesticides, timber preservatives, and electronics production	10	Keratosis, skin cancer, and internal organ cancer	88 and 121–125
Cadmium (Cd)	Electroplating, battery, petroleum products, and synthetic chemicals	3	Lung, breast, prostate, pancreas, urinary bladder, and nasopharynx cancers	126 and 127
Mercury (Hg)	Iron and steel industry and chloro-alkali industry	6	Itai-itai disease, renal injury, cardiovascular disease, and myocardial infarction	86 and 128–132
Lead (Pb)	Mining, smelting, waste incineration, coal burning, leaded gasoline, dust, batteries vent, and lead paint	10	Saturnism or plumbism, mainly affecting the gastrointestinal and nervous systems and severe damage to the brain and kidneys	133–136
Chromium (Cr)	Metallurgy, electroplating, production of paints and pigments, tanning, and wood preservation	50	Lower IQ, hearing loss, anemia, kidney failure, blindness, hallucination, cardiovascular disorder, impair development, allergic contact dermatitis, cardiovascular disorder, hepatotoxicity, and respiratory infections	137 and 138
Nickel (Ni)	Ni alloy industry, pigment manufacturing industries, and tannery industry	70	Allergic contact dermatitis, cardiovascular disorder, hepatotoxicity, and respiratory infection	139–143
Cobalt (Co)	Coloring agent for glass, pottery, and jewelry	50	Cardiomyopathy, occupational asthma, allergic alveolitis, and occupational contact dermatitis	144–146

Table 2 Compilation of conventional techniques employed for heavy metal detection including their respective limits of detection (LODs)

Heavy metals	Technique	Limit of detection	Reference
Mercury (Hg)	Atomic absorption spectroscopy (AAS)	0.0155 μg L^{-1}	15
	Atomic fluorescence spectrometry (AFS)	Hg^{2+} – 0.007 μg L^{-1} CH_3Hg^+ – 0.018 μg L^{-1}	16
	Graphite Furnace Atomic Absorption Spectrometry (GF-AAS)	Hg – 0.017 μg L^{-1}	147
	SWASV	0.1 μg L^{-1}	148
	ICP-MS	0.09 ng g^{-1}	17
Lead (Pb)	GF-AAS	Pb – 0.009 μg L^{-1}	147
	ICP-MS	0.031 ng L^{-1}	149
	Potentiometry	31 μg L^{-1}	150
	Amperometry	2 ppb	151
	High resolution continuum source graphite furnace atomic absorption spectrometry (HR-CS-GFF-AAS)	200 ng L^{-1}	152
Arsenic (As)	ICP-MS	As(III) – 0.008 μg kg^{-1} As(V) – 0.013 μg kg^{-1}	28 and 153
	Cyclic voltammetry	4.64 μM	154
	Differential pulse anodic stripping voltammetry (DPASV)	11.39 pM	155
Cadmium (Cd)	HR-CS-GFF-AAS	100 ng L^{-1}	152
	SWASV	0.062 ppb	156
	AFS	0.05 μg L^{-1}	157
	ICP-MS	0.008 μg L^{-1}	158
Nickel (Ni)	ICP-MS	1.2 pg mL^{-1}	159
	AAS	0.305 μg L^{-1}	160
	GF-AAS		
Chromium (Cr)	Flame atomic absorption spectrometry (FAAS)	0.21 μg L^{-1}	161
	Ion chromatography-inductively coupled plasma-mass spectrometry (IC-ICP-MS)	Cr(III) – 0.09 μg L^{-1} Cr(VI) – 0.03 μg L^{-1}	162
	Amperometry	0.0016 μM	163

conventional techniques, microfluidics provides faster reaction time, minimum waste generation, and reduced sample and reagent consumption. Microfluidic devices have found applications in various research fields, including chemistry,[27] microelectronics,[10] material biology,[28] biomedical engineering,[29] and fluid dynamics.[30]

Microfluidic devices can be fabricated using different types of materials such as glass,[31] silicon,[32] polydimethylsiloxane (PDMS), thermoplastics,[33] paper,[34] *etc.* Silicon was the first material used in the fabrication of microfluidic channels.[35] The surface of silicon is made up of silanol groups (–Si–OH–) which can be easily modified. Its semiconducting properties, chemical resistance and flexibility made silicon one of the most widely used materials in fabrication.[36] Silicon glass was the most widely used material in microfluidic devices due to its properties such as high transparency, low fluorescence background,[37] and high resistance to temperature (>500–1500 °C).[38] However, fabrication of glass and silicon based microfluidic devices requires a cleanroom facility which makes fabrication expensive. It also requires the use of hazardous chemicals such as HF. Consequently, this has limited the use of glass and silicon.[39,40] PDMS is the most common type of elastomer used in the fabrication of microfluidics because of its high elasticity, cost-effectiveness and simple fabrication steps.[41] PDMS enables fabrication of multilayered microchannels by stacking multiple layers.[42] However, PDMS shows certain drawbacks such as incompatibility towards certain organic solvents and adsorption of biomolecules due to its hydrophobic properties.[43,44] Thermoplastics show better solvent compatibility compared to PDMS. They include polystyrene (PS), polyethylene terephthalate (PET), polyvinyl chloride (PVC) and polymethyl methacrylate (PMMA).[45] However, the major drawback of thermoplastics is their inability to adhere to other surfaces.[46] Paper is one of the cheapest, portable, nature friendly, highly porous cellulose based materials, and is widely used as a microfluidic material.[47] The capillary movement of a liquid along a paper-based microfluidic device liquid simplifies the fabrication of microchannels.[48] The major limitation of paper is its reusability, as it can be used only once. The selection of material for fabrication depends upon the type of samples used, nature of chemical reagents and application. Microfluidic devices exhibit some unique features compared to macroscale devices, such as a high surface-to-volume ratio and laminar flow; hence, the selection of suitable materials for the fabrication of microfluidic devices is crucial. Various types of sensors, such as electrochemical, optical, hybrid, and biosensors, are integrated into microfluidic devices to detect heavy metals.

Optical detection

The detecting components react with the analyte resulting in optical variations, which is identified by optical detection. This method is a basic, cost-effective technique that uses electromagnetic radiation with wavelengths ranging from 200 nm to 1 mm. The electromagnetic domain is further divided into the UV, visible, and near-infrared regions.[49] The widely used optical

detection methods include colorimetry, absorbance-based detection and fluorescence detection. Heavy metals will interact with chemical reagents that exhibit optical properties, including nanoparticles, fluorescent proteins, synthetic dyes, and quantum dots. The optical signal will undergo changes due to the interaction between these chemical reagents and varying concentrations of heavy metals, enabling the quantification of each heavy metal through recorded measurements.[50] Metallic nanoparticles such as AuNPs and AgNPs exhibit a phenomenon known as SPR, which is used for heavy metal detection. SPR is widely used due to its specific features, such as sensitivity toward the detection of analytes under very dilute conditions, high selectivity, and label-free sensing.[51,52] SPR is a quantum optical-electrical occurrence that occurs during the interaction of light and metal surfaces. This technique involves generation of plasmonic waves between the metal layer and the dielectric medium.[22] It employs singular and p-polarized light to generate surface plasmons. As the momentum of the SPR wave matches that of the incoming light, the intensity of the reflected light starts to diminish because of the resonance. The angle at which the intensity diminishes is called the resonance angle. The resonance angle is determined by the refractive index of the metal surface.[52] The intensity of the reflected light starts to diminish due to resonance photons from incident light at a specific angle of incidence called the resonance angle, exciting the electrons on the metal surface layer, which upon excitation propagate in a direction parallel to the metal surface.[23]

Colorimetry detection

Heavy metal detection utilizing microfluidics and colorimetry is a semiquantitative process. In colorimetric detection, the chemical reaction between the solution or the substrate containing the heavy metal and the chemical reagent employed for its detection results in a colour change which can be observed for confirming the presence of the heavy metal, and the concentration can be determined using an optical system. Specific dyes or chemical reagents for the metal are employed when detecting various heavy metals in water.

Development of a paper-based microfluidic device for detecting Pb^{2+} using the colorimetric method was reported by Wisang *et al.* The device consisted of two zones: a sample zone and a detection zone. To indicate the presence of Pb^{2+}, sodium rhodizonate was employed as the indicator. When Pb^{2+} was introduced to sodium rhodizonate, the colour changed from yellow to pink because of the formation of a Pb–rhodizonate complex. The limit of detection (LOD) was found to be 0.756 mg L^{-1} (756 ppb) (Fig. 2).[22]

Substituting the need for individual devices that are specific to different heavy metals with a single device capable of simultaneously detecting multiple heavy metals is both cost-effective and time saving. A paper-based microfluidic device for simultaneous detection of Ni^{2+}, Cu^{2+} and Fe^{2+} was developed by Aryal *et al.* for the substrate Whatman grade 1 was used with five folds. The top three layers of the fold were used as detection pads, and the bottom two layers were used as waste pads. The detection of Ni^{2+} was achieved using Chugaev's method; briefly,

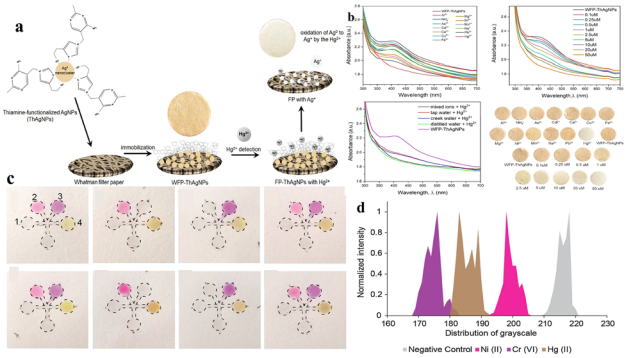

Fig. 2 (a) A schematic representation of the possible mechanism involved in the detection of Hg^{2+} through a color change using ThAgNPs anchored on filter paper. (b) UV-vis spectra of WFP-ThAgNPs exposed to different ions and various concentrations of Hg^{2+} (reproduced from Budlyan *et al.*, 2022, *Environmental Nanotechnology, Monitoring and Management*).[57] (c) μPAD showing the color development after the application of DI water, 5 ppm of Ni^{2+}, Cr^{6+}, or Hg^{2+}, and heavy metal ion spiked lake-water samples. (d) Graphical representation of the distribution of grayscale *vs.* normalized intensity (reproduced from Devadhasan and Kim, 2018, with permission from Elsevier).[54]

it involved the reaction of Ni^{2+} ions with dimethylglyoxime (DMG), a bidentate organic ligand, in the presence of alkaline ammonium solution. A pink-colored complex known as nickel dimethylglyoxime (NiDMG2) was formed as a result of the reaction. Cu^{2+} was identified using a precise and highly responsive Cu–bathocuproine test. An orange-colored compound was formed when Cu^{2+} interacted with bathocuproine in an acidic environment (pH 4.5). Fe^{2+} was identified utilizing bathophenanthroline. Under acidic conditions (pH 4.5), bathophenanthroline reacts with Fe^{2+} to produce a complex with a red color. The LODs of Ni^{2+}, Cu^{2+} and Fe^{2+} were found to be 2 ppm (2000 ppb), 6.67 ppm (6670 ppb), and 1 ppm (1000 ppb), respectively.[53] Multiple heavy metals, such as Ni^{2+}, Cr^{3+}, and Hg^{2+} were detected by the paper-based microfluidic device. The substrate was a chromatographic paper with detection zones for three different heavy metals. The surface of each detection zone was functionalized with three different functional groups: amine ($-NH_2$), carboxyl (–COOH), and thiol (–SH). The substrate was subjected to chemical reactions for the immobilization of these functional groups on its surface. The immobilization of the functionalized groups was followed by the addition of heavy-metal-specific colorimetric reagents such as dimethylglyoxime, 1,5-diphenylcarbazide, and Michler's thioketone to this detection zone for the detection of Ni^{2+}, Cr^{3+} and Hg^{2+} respectively. The interaction of the chemical reagent with the heavy metals resulted in the development of bluish-purple, orange, and yellow colours, which were analyzed using the colours developed by standard solutions; analysis of the images was performed to obtain the grayscale for quantification. The LODs of Ni^{2+}, Cr^{3+}, and Hg^{2+} were found to be 0.24 ppm (240 ppb), 0.18 ppm (180 ppb), and 0.19 ppm (190 ppb), respectively.[54] Even though the use of colorimetric assays or dyes in optical detection of heavy metals is easy, economically effective, and rapid, these assays tend to lack sensitivity due to inherent

limitations in the low extinction coefficients of the dyes.[55,56] The sensitivity of detection can be improved by using nanosized particles of gold (AuNPs) and silver (AgNPs). The aggregation of the nanoparticles by heavy metals can be associated with their optical and surface plasmon resonance (SPR) characteristics. The change of colour in the solution due to the aggregation of nanoparticles enhances the sensitivity of this method of detection. Budlayan *et al.* used thiamine functionalized AgNPs in the detection of Hg^{2+}. Thiamine-functionalized AuNPs were immobilized on filter paper. Thiamine shows selective coordination with Hg^{2+}, and the AgNPs demonstrate highly adjustable optical absorption and reactivity. When the Hg containing water sample is poured on the Whatman filter paper with thiamine functionalized AuNPs, a colour change from yellow to faint yellow to white is observed, and the changed intensity corresponds to the quantity of tested Hg^{2+}. The change in the colour of the filter paper was a result of a reduction in the absorbance peak at approximately 425 nm in the UV-vis spectrum. ImageJ software was utilized to assess the red, green, and blue (RGB) colour intensity profiles of the obtained digital images. This characterization method offers a semiquantitative assessment of the colorimetric response. High intensities were recorded from red and green colors, resulting in the yellow color of the filter paper. The LOD of this sensor was found to be 0.5 μM (0.5 ppb).[57] In their study, Sahu *et al.* employed glucose-functionalized AuNPs to detect As^{3+} and Pb^{2+}. The presence of As^{3+} and Pb^{2+} was detected by glucose-functionalized AuNPs with a change in color from pink to purple and bluish gray, respectively. The change in colour due to the interaction of glucose-functionalized AuNPs with the heavy metals can be visualized through the naked eye. To measure the intensity of this change in colour, a UV-vis spectrometer was used. The limit of detection of As^{3+} and Pb^{2+} was found to be 5.6 μg L^{-1} and 7.7 μg L^{-1}, respectively.[58] Despite its simplicity, rapidity, and portability as a method for detecting heavy metals, colorimetry is considered a basic detection approach due to its semiquantitative nature and limitations in terms of the LOD. Table 3 provides a summary of the various microfluidic-based devices used for heavy metal detection using colorimetry.

Absorbance-based detection

In absorbance-based detection, light-emitting diodes (LEDs) and LASER (Light Amplification by Stimulated Emission of Radiation) are used as a light source. LEDs have high durability, low cost, low power consumption, high energy conversion efficiency, small size, and broad spectral band from UV to NIR, which makes them some of the most frequently used light sources in optofluidic detection of heavy metals.[59] LED-based sensors eliminate the need for optical couplers or monochromators because LEDs emit a relatively narrow range of wavelengths. Additionally, LEDs can be easily electronically modulated for intensity, eliminating the necessity for a separate mechanical chopper. Light from the light source enters the device's microchannel, where the light and the heavy metals in water interact. The light will be absorbed by the metal ions, which then emit at different intensities recorded by the detectors.[60]

Lace *et al.* used a green dye, leucomalachite, for the detection of As^{3+} using optical detection where the LED was used as a light source with a photodiode detector (Fig. 3). The microfluidic device was made up of poly(methyl methacrylate) (PMMA). The chip was made up of serpentine channels used for the mixing of the reagents. The reaction of dye with As^{3+} produced a green-

Table 3 Different colorimetry-based techniques in heavy metal detection

Heavy metals	Microfluidic device	Indicator	LOD	Reference
Pb^{2+}	Paper-based	Sodium rhodizonate	756 ppb	22
Ni^{2+}, Cu^{2+} and Fe^{2+}	Paper-based	Dimethylglyoxime (DMG) Bathocuproine Bathophenanthroline	Ni^{2+} – 2000 ppb Cu^{2+} – 6670 ppb Fe^{2+} – 1000 ppb	53
Ni^{2+}, Cr^{3+}, and Hg^{2+}	Paper-based	Dimethylglyoxime, 1,5-diphenylcarbazide, and Michler's thioketone	Ni^{2+} – 240 ppb Cr^{3+} – 180 ppb Hg^{2+} – 190 ppb	54
Hg^{2+}	Paper-based	Thiamine functionalized AgNPs	0.5 ppb	57
As^{3+} and Pb^{2+}	Paper-based	Glucose-functionalized AuNPs	As^{3+} – 5.6 μg L^{-1} Pb^{2+} – 7.7 μg L^{-1}	58
Cu^{2+}	Paper-based	Chrome azurol S and pyrocatechol violet	Chrome azurol S – 1700 ppb Pyrocatechol violet – 1900 ppb	164
Cu^{2+}, Co^{2+}, Ni^{2+}, Hg^{2+}, Mn^{2+}	Paper-based silver nanoparticles were modified with pyrrolidine-1-dithiocarboxylic acid ammonium salt	Bathocuproine (BC) Dimethylglyoxime (DMG) Dithizone (DTZ) 4-(2-Pyridylazo)resorcinol (PAR)	Cu^{2+} – 320 ppb Co^{2+} – 590 ppb Ni^{2+} – 5870 ppb Hg^{2+} – 200 ppb Mn^{2+} – 110 ppb	165
Cr^{3+} and Al^{3+}	PMMA	AgNPs modified with pyrrolidine-1-dithiocarboxylic acid ammonium salt	Cr^{3+} – 0.010 ppb Al^{3+} – 0.003 ppb	166
Ni^{2+}, Cu^{2+}, Cr^{6+}	Paper-based	Ni^{2+} – dimethylglyoxime Cu^{2+} – bathocuproine Cr^{6+} – 1,5-diphenylcarbazide	Ni^{2+} – 4.8 mg L^{-1} Cu^{2+} – 1.6 mg L^{-1} Cr^{6+} – 0.18 mg L^{-1}	167

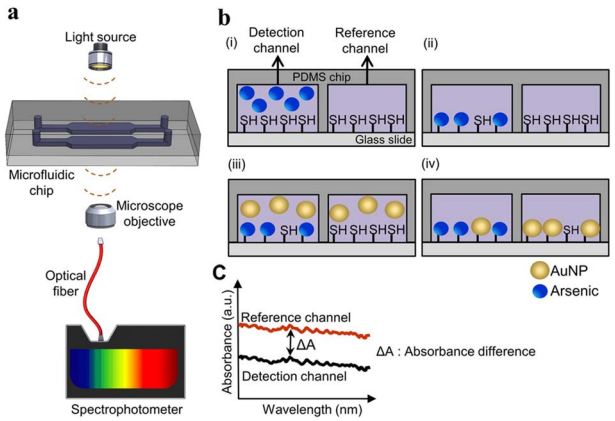

Fig. 3 Detection of As(III) in the microfluidic chip. (a) Representation of a microfluidic device in As(III) detection; (b) illustration of the As(III) detection procedure: (i) injection of As into the detection channel and injection of reference solutions into reference channels, (ii) washing of the channel with distilled water, (iii) introduction of AuNPs in the microchannels and (iv) washing of the microchannels; (c) measurement of absorbance from the reference channel and detection channel containing As and reference solutions, respectively. The difference in absorbance in the channel was used to calculate the concentration of As (reproduced from Karakuzu *et al.*, 2021, with permission from Elsevier).[62]

colored complex, giving an absorption peak at 617 nm. The LOD was found to be 0.19 mg L^{-1}. A method was developed to detect As^{3+} using iron oxide nanoparticles by Chauhan *et al.*, where the iron oxide surface was modified with cysteine. A filter paper with a hydrophobic zone was used as the substrate where the cysteine-modified iron oxide nanoparticles reacted with As^{3+}. The LOD was found to be 10 ppb.[61] A polydimethylsiloxane (PDMS)-based microfluidic device for the detection of Hg^{2+} was developed by Li and Lin. In this device, an LED served as the light source with a wavelength of 525 nm, while a photomultiplier functioned as the detector. For precise detection of Hg^{2+}, the AuNPs were modified with 3-mercaptopropionic acid (3-MPA), leading to aggregation of AuNPs. A UV-vis spectrophotometer was used to quantify Hg^{2+}, revealing an LOD of 200 ppb.[27] To identify a specific heavy metal from a mixture of heavy metals in water, metal-specific compounds or reagents can be used.[27,61] A microfluidic device where the microchannels were modified with –SH groups was developed by Karakuzu *et al.* The As from the water source adhered to these –SH groups, with unaltered AuNPs serving as markers that bind to free –SH groups. The intensity of absorbance recorded at 530 nm, for the AuNPs was inversely proportional to the As concentration. The LOD was determined to be 2.2 μg L^{-1} (2.2 ppb).[62] Table 4 provides an overview of optical-based microfluidic devices for detecting heavy metals.

Fluorescence-based detection

Fluorescence-based detection of heavy metals is one of the simplest methods with high sensitivity and fast response time. Fluorescence detection involves the emission of higher wavelength light from the sample surface after it has been exposed to low wavelength light. As the concentration of the analyte increases, the intensity of light decreases. Typically, in this approach, fluorescent probes are combined with the analyte of interest. Various probes are employed for fluorescence detection. The analyte can be detected as the fluorescence signal alters upon the attachment of the probe to the specific analyte. The fluorescent probes can be further classified based on their optical performance into "off–on" probes and "on–off" probes. The binding of fluorescent probes to analytes may enhance the fluorescence (off–on) or quench the fluorescence (on–off). Rhodamine dye and its derivatives exhibit longer excitation wavelengths, high fluorescence quantum yield, and high photostability, rendering them the prevailing choice for fluorescent

Table 4 Absorbance-based heavy metal detection

Heavy metal	Type of detection	Device	LOD	Reference
As^{3+}	Absorbance based detection	PMMA	190 ppb	61
As^{3+}	Absorbance based detection	PDMS	10 ppb	99
Hg^{2+}	Absorbance based detection	PDMS	200 ppb	27
As^{3+}	Absorbance-based	PDMS	2.2 ppb	62
Hg^{2+}	Fluorescence	PDMS	2 nM	66
Cr^{3+}	Fluorescence	PDMS	0.094 nM	67
Hg^{2+} and Pb^{2+}	Fluorescence	PDMS	Hg^{2+} – 0.70 ppb Pb^{2+} – 0.53 ppb	69
Cu^{2+}, Mn^{2+}, and Hg^{2+}	Fluorescence	Paper-based	Hg^{2+} – 5.4 nM Mn^{2+} – 8.1 nM Cu^{2+} – 7.3 nM	72
Cd^{2+}	Fluorescence	PDMS	0.26 μg L^{-1}	77
Hg^{2+} and Pb^{2+}	Fluorescence	Cloth-based	Hg^{2+} – 0.18 ppb Pb^{2+} – 0.07 ppb	73
Cd^{2+} and Pb^{2+}	Fluorescence	Paper-based	Cd^{2+} – 0.245 ppb Pb^{2+} – 0.335 ppb	76
Hg^{2+}	LSPR	PDMS	2.7 pM	87

probes. Rhodamine and its derivatives are being used in detecting heavy metals like Cd^{2+} and Pb^{2+}, Cd^{2+} and Hg^{2+}.[63–65]

A PDMS-based microfluidic device was fabricated by Karthikeyan and Sujatha for the detection of Hg^{2+} where the fluorescent sensing probe was a gold nanofluid surface functionalized with rhodamine 6G and L-arginine amino acid. The device was incorporated with two inlets and an outlet for fluid entry and exit, respectively. The device was also incorporated with a herringbone type of micromixer that enabled the mixing of the fluids. The analysis of Hg^{2+} with a concentration of 0–16 nM showed an increase in fluorescence intensity as the concentration of Hg^{2+} increased. The maximum detectable concentration of Hg^{2+} was found to be 16 nM, beyond which the intensity decreased. The LOD was determined to be 2 nM.[66] Peng *et al.* used rhodamine B derivatives for the detection of Hg^{2+}. For simultaneous analysis of the fluorescence intensity, a portable fibre-optic spectrophotometer was coupled with a fabricated microchip. 0.094 nM was the LOD found.[67] The accuracy and sensitivity of heavy metal detection can be improved using fluorescent aptamers. Aptamers are target-specific DNAs or RNAs that show excellent stability compared to antibodies; therefore, they can be utilized in heavy metal detection. For example, thymine (T) nucleotides show greater specificity toward Hg^{2+} than other heavy metals.[68] Similarly, Pb can be detected using quadruplexes. Fluorescent sensors coupled with aptamers were used for sensitive detection of Hg^{2+} and Pb^{2+}. Fluorescent dyes such as FAM and HEX were used in the labelling of the aptamer sequences and mixed with GO solution and 500 ppm of heavy metals. The fluorescence produced by FAM and HEX was quenched by GO. The interaction of Hg^{2+} and Pb^{2+} with the aptamer led to the restoration of fluorescence. An increase in fluorescence was observed with an increase in heavy metal concentration with a LOD of 0.70 ppb and 0.53 ppb for Hg^{2+} and Pb^{2+}, respectively.[69]

Zero-dimensional particles with dimensions of 2–100 nm, called quantum dots (QDs) can also be used as nanosensors. QDs show unique properties, such as wide absorption ranges, precise and adjustable emission ranges, extended fluorescence duration, exceptional resilience to light-induced decay, and resistance to photodegradation, making them an alternative for organic and protein fluorescent dyes.[70] A paper-based device (PAD) by Yue *et al.* uses QDs for detection of heavy metals such as Cu^{2+}, Mn^{2+}, and Hg^{2+} by the colorimetric technique of detection. The PAD consists of three different layers, a sample area, three channels, and a testing area. The different testing areas were surface-modified with *O*-phenylenediamine (OPD), sodium 3-(*N*-ethyl-3-methylanilino)-2-hydroxypropanesulfonate (TOOS), 4-aminoantipyrine (4-AAP) mixture, and 3,3′,5,5′-tetramethylbenzidine (TMB) followed by the addition of C-NH_2QDs, C-COOH QDs and CdSe QDs. The concentrations of Hg^{2+}, Mn^{2+}, and Cu^{2+} were determined by photocatalytic oxidation of TMB, the TOOS-4-AAP mixture, and OPD using C-COOH QDs, CdSe QDs, and NH_2QDs, respectively. After the reaction, using the photo of the PAD, the testing areas were analysed. The LODs of Hg^{2+}, Mn^{2+}, and Cu^{2+} were found to be 5.4 nM, 8.1 nM, and 7.3 nM, respectively. CdTe/CdS QDs have applicability in the detection of Cd^{2+}.[71] A three-dimensional origami ion imprinted polymer paper-based microfluidic device was developed for the detection of Cu^{2+} and Hg^{2+}. The fluorescence quenching mechanism was employed through formation of Cu^{2+} or the Hg^{2+} IIP and CdTe QD complex, where there was a transfer of photo luminescence energy of QDs to the complex. The platform enabled simultaneous detection of Cu^{2+} and Hg^{2+} with a LOD of 0.11 μg L^{-1} to 58.0 μg L^{-1}.[72] Similarly, a cloth/paper hybrid was used as a substrate for detection of Hg^{2+}, Pb^{2+} and Cr^{6+} using QDs. The device was integrated with a fluorescent sensing cloth-based component and paper-based μPAD. The sensing component of the device was prepared by grafting the QDs on the surface of the cloth followed by the modification with ion imprinted polymers (IIPs). The detection of Hg^{2+} and Pb^{2+} was carried out using fluorescence quenching. The LOD achieved was found to be 0.18 μg L^{-1} for Pb^{2+} and 0.07 μg L^{-1} for Hg^{2}.[73] Wang *et al.* used tetrasodium iminodisuccinate (IDS) in the etching of CdTe/CdS QDs. Chemical etching caused fluorescence quenching of the CdTe/CdS QDs, enabling sensing of Cd^{2+} ions and consequent alterations in fluorescence emission. These changes were captured by a fluorescent E-eye comprising an excitation source, an optical lens, and a smartphone. The LOD achieved in this study was determined to be 0.26 μg L^{-1}.[74] The uniform distribution of QDs on the substrate can be achieved by grafting onto the surface of the nanoparticles. In the study by Han *et al.* the QDs were grafted onto the surface of the silica nanoparticles and the uniform distribution was achieved. The grafted QDs were used in the detection of Hg^{2+} in water. The Hg^{2+} was detected using fluorescence quenching of QDs. The fluorescence signals were captured using a smartphone and grayscale data were obtained. The LOD was found to be 2.83 μg L^{-1}.[75] Although CdTE/CdS QDs are sensitive in fluorescence detection, they are highly toxic to the environment. ZeSe QDs show less toxicity than CdTe QDs. Hence, Zhou *et al.* used ZnSe QDs for the detection of Cd^{2+} and Pb^{2+} ions. The microfluidic device used was known as 3D rotary μPADs modified with ZnSe QD-wrapped ion-imprinted polymers. The LODs of Cd^{2+} and Pb^{2+} were found to be 0.245 μg L^{-1} and 0.335 μg L^{-1}, respectively.[76] A rhodamine B-graphed paper-based microfluidic device was fabricated by Liu *et al.*, 2022 to detect Fe^{3+}. The addition of Fe^{3+} to the device changed the colour from colourless to pink, whereas the addition of other heavy metals, such as Pb^{2+}, Cu^{2+}, Ni^{2+}, and Hg^{2+}, did not result in any significant colour change (Fig. 4).[83]

Electrochemical detection

The electrochemical method of heavy metal detection is a strong alternative due to its various advantages, such as selectivity toward metals, broader linear dynamic range, high sensitivity[78] portability, and easy sample preparation steps.[79] In electrochemical detection, the analytes interact with the electrode or probe, producing electrical signals.[80] There are three kinds of electrodes in the electrochemical technique, the working electrode (WE), counter electrode (CE), and reference electrode (RE). The WE generate measurable current, potential, charge, or frequency differences as a result of the electrochemical reaction.[10] The fabrication of the electrochemical

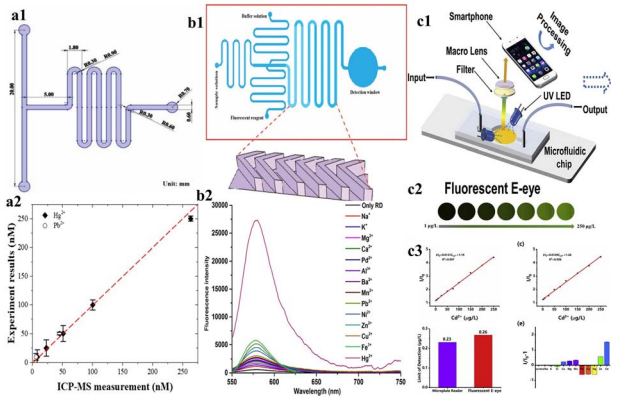

Fig. 4 (a1) Schematic representation of the microchannel of the microfluidic device; (a2) Graphical representation of a comparison of results obtained by ICP-MS and the microfluidic device (reproduced with permission from Huang *et al.*, 2021);[69] (b1) schematic representation of a microchannel; (b2) graphical representation of fluorescence intensity of various heavy metals (reproduced with permission from Peng *et al.*, 2018);[67] (c1) schematic representation of a procedure for Cd^{2+} detection using a fluorescent E-eye with QDs; (c2) FL images of different concentrations of Cd^{2+} by using a fluorescent E-eye; (c3) the calibration curve for different concentrations of Cd^{2+} using a microplate reader and fluorescent E-eye (reproduced from Wang *et al.*, 2020, with permission from Elsevier).[77]

electrode is important. Frequently, electrode fabrication involves the hybridization of two or more materials. These include materials with improved conductivity to facilitate electron transmission, materials with high porosity that provide a larger surface area containing a large number of active sites for the binding of active components or heavy metals and materials containing the functional group on the surface area that enhance metal attachment and selectivity for a particular target metal ion. The most common materials used include carbon-based materials, bismuth-based materials, and polymer-based materials.[81,82] Carbon nanotubes (CNTs), graphene, and fullerenes are some of the carbon-based materials.[25] Carbon nanomaterials are considered the most versatile materials that are environment friendly. They possess specific properties like high electrical conductivity and high stability, and the surface of carbon can be easily modified.[82] A low-cost disposable graphene-based sensor for the detection of heavy metals such as Cd^{2+}, Cu^{2+} and Pb^{2+} was developed by Yue *et al.* The WE, RE, and CE were graphene-ferrocene-doped graphene and Chit-Fc, respectively.[71]

Bismuth shows minimal toxicity and is hence regarded as one of the best choices for a heavy metal sensor. It is partially insensitive to dissolved oxygen (DO). Hwang *et al.* developed a modified nanoporous bismuth electrode (modified-NPBiE) for the detection of heavy metals such as Cd^{2+} and Pb^{2+}.[84] Printed electrochemical sensors are considered economical analytical detection methods for single-use and disposable sensors.[85] The advancement of microelectronics resulted in the easy accession of electrochemical sensors. Inkjet printing, 3D printing, and screen printing are the most common methods for printing electrodes and are widely employed to create planar electrodes for electrochemical sensing.[86,87] Screen-printed electrodes (SPEs) are single-use electrodes that are cost-effective and are fabricated in large quantities. These electrodes are user-friendly and do not require any preprocessing or specialized personnel.[88] The steps involved in the fabrication are as follows: transfer of electrode design onto the substrate, mask creation by eliminating the undesired sections of the mask, application of the electrode ink onto the mask followed by drying, and finally, removal of the mask to acquire electrodes of its shape.[89] The fundamental constituents of conductive screen-printing ink include solvents, conductive nanoparticles, organic binders, and conductive agents.[90] Electrode sensitivity can be improved by integrating modified substances into the printing ink. These include inorganic materials such as gold, silver organic materials such as chitosan, carbon-based materials such as graphene, and carbon nanotubes.[91] Inkjet printing is one of the most common techniques in microstructure fabrication and involves a dispensing unit for the deposition of liquid material on the surface of the substrate. The major advantages of inkjet printing include uniform deposition of the material on the substrate, maskless fabrication of electrodes, minimum sample consumption, and cost-effectiveness.[92,93] Ink-jet printing is an automated process that digitally manages the deposition of ink on predetermined spots on a substrate. This process enables exceptional accuracy, ensuring consistent reproducibility of the printed electrodes.[94] The distinct designs of the electrodes were created using graphic design software and are printed. The sensitivity of detection can be improved by mixing the biomolecules or nanomaterials with the printing ink.[85] The limitation of the fabrication of a single layer of the electrode by inkjet printing was resolved by adopting 3D inkjet printing, enabling the production of multiple layers of electrodes. The advantages of 3D printing include large-scale manufacturing capabilities, personalized electrode design, and streaming of the fabrication process into a single step.[95,96] The classification of different electrochemical techniques involved in heavy metal detection is shown in Fig. 5.

Among these techniques, the most widely used electrochemical techniques for heavy metal analysis are potentiometry, amperometry, and voltammetry techniques. The potentiometric method is based on the continuous measurement of the potential difference between the electrodes, which, in turn, facilitates the quantification of analyte concentrations.[98] Potentiometry-based detection is a simple technique

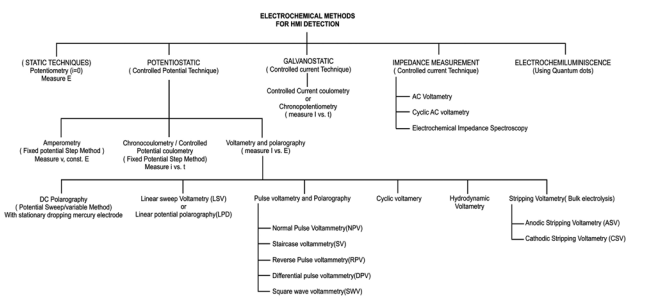

Fig. 5 List of different electrochemical-based techniques (reproduced from Bansod *et al.*, 2017, with permission from Elsevier).[97]

that is widely used because of its cost-effectiveness and high selectivity. Voltammetry techniques are widely adopted in microfluidic-based heavy metal detection due to their sensitivity, simplicity, and ability to provide real-time electrochemical information about analytes.[99] These techniques involve applying a potential across the electrodes and measuring the resulting current, allowing for the characterization and quantification of various electroactive species, including heavy metal ions.[97] In microfluidics, these techniques are particularly advantageous as they can be integrated with miniaturized devices, enhancing sensitivity and reducing sample and reagent consumption. Here is a brief overview of some common techniques used in microfluidic-based heavy metal detection:

- **Cyclic voltammetry (CV).** Cyclic voltammetry involves sweeping the potential applied to an electrode over a range of values and measuring the current produced. This technique provides information about the redox behavior of analytes, including oxidation and reduction potentials.[100] In microfluidics, CV can be incorporated into lab-on-a-chip systems, enabling rapid and real-time heavy metal analysis. The technique is suitable for studying multiple redox-active heavy metals simultaneously.[101]
- **Square wave voltammetry (SWV).** SWV is a pulsed technique that involves the application of a series of potential pulses to an electrode.[102] It provides enhanced sensitivity and reduced background noise compared to cyclic voltammetry. In microfluidics, SWV can be utilized to detect heavy metal ions with high sensitivity, making it suitable for trace analysis in environmental samples.[103]
- **Stripping voltammetry (ASV and CSV).** ASV and CSV are techniques that are used in enhancing the detection of trace-level analytes.[104] They involve preconcentration of analytes on the surface of the electrode followed by the measurement of stripping peak current using a voltammetric scan.[105] In microfluidics, these techniques can be combined with microelectrodes to achieve high sensitivity even in small sample volumes.[106]
- **Differential pulse voltammetry (DPV).** This technique provides improved sensitivity by subtracting the capacitive current and background noise from the measured current.[107] It is mainly useful for analysis of complex samples. In microfluidics, DPV can be implemented to detect heavy metal ions in a controlled and precise manner.[108]
- **Amperometric detection.** While not a traditional voltammetry technique, amperometry detection is closely related. It involves the measurement of current produced when a constant potential is applied between the working and reference electrodes. Amperometric sensors can be integrated into microfluidic devices to detect heavy metal ions based on changes in current resulting from analyte interactions with the sensor surface.[109]

Microfluidics allows for precise control of fluid flow, which is crucial for electrochemical measurements. Microfluidic channels can be designed for enhancing the mass transport to the electrode surface, improving the sensitivity and response time of voltammetry techniques.[110] Additionally, microfabrication techniques can be employed to create miniaturized electrodes and electrode arrays, enhancing the analytical capabilities of these techniques.[111] Microfluidic-based voltammetry offers several advantages that include minimum usage of the sample and reagent, rapid analysis, and the potential for automation and integration with other analytical techniques.[112] It has been successfully applied to heavy metal detection in various environmental samples, including water, soil, and biological fluids. However, challenges such as electrode fouling and interference from complex matrices still need to be addressed for accurate and reliable heavy metal quantification in real-world samples. Certainly, there are a few scientific studies that demonstrate how voltammetry techniques are employed in microfluidic-based heavy metal detection. Kokkinos *et al.* developed a paper-based electrochemical device with tin (Sn) as the WE, platinum (Pt) as the CE, and silver (Ag) as the RE. The device was integrated with a microfluidic channel, and the three electrodes were deposited onto the paper substrate using a sputtering process. The developed device was used in the voltammetric detection of Cd^{2+} and Zn^{2+} using ASV. The LOD was found to be 0.9 ppb and 1.1 ppb for Cd^{2+} and Zn^{2+} respectively (Fig. 6).[113]

Mohan *et al.* fabricated a microfluidic electroanalytical device for simultaneous detection of Cu and Hg. The device was fabricated using maskless lithography where PDMS was used as the substrate. ITO was used as the WE and CE, and Ag/AgCl deposited on the tip of the third ITO electrode was used as the RE. The device was connected to a portable potentiostat and smartphone. Hg and Cu underwent oxidation at −0.4 V and 0.1 V, respectively. The device was tested with samples of tap water, lake water, and blood. The LODs of Cu and Hg were 0.4 μM and

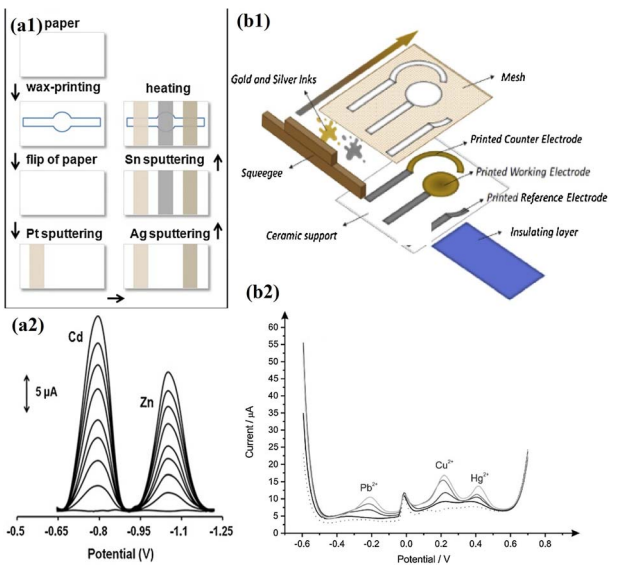

Fig. 6 (a1) Schematic representation of steps involved in fabrication of an ePAD; (a2) SWASV voltammogram of Zn^{2+} and Cd^{2+} (0–40 μg L^{-1}) (reproduced with permission from Kokkinos *et al.*, 2018);[113] (b1) schematic representation of the fabrication of a screen-printed electrode. Schematic representation of steps involved in the fabrication of ePADs; (b2) SWASV voltammograms and calibration plots of 0–40 μg L^{-1} Zn^{2+} and Cd^{2+} (reproduced from Bernalte *et al.*, 2020, with permission from Elsevier).[114]

3.19 μM, respectively.[115] Santangelo *et al.* introduced an innovative technique for the electrochemical analysis of heavy metals, which involved a graphene-based sensor integrated with a 3D-printed microfluidic chip. EG/SiC, Ag/AgCl, and Pt were used as the WE, CE, and RE, respectively. A portable potentiostat was used for the electrochemical analysis. The developed device was used for the detection of Cd^{2+} and Pb^{2+}.[116] Subramanian *et al.* developed a microfluidic device integrated with a radial microchannel to electrodes. Linear sweep voltammetry was conducted for the detection of various heavy metal ions. The LOD of As^{3+} was found to be 1 ppb. Specific peaks for Cu^{2+}, Fe^{2+}, Mn^{2+}, and Pb^{2+} were also observed in the voltammogram.[117] A point-of-care testing (POCT) electrochemical-based device was developed by Xu *et al.* for the simultaneous detection of multiple heavy metals, such as Cd^{2+}, Cu^{2+}, Hg^{2+} and Pb^{2+}, using DPV. The LODs for Cd^{2+}, Cu^{2+}, Hg^{2+} and Pb^{2+} were found to be 0.29 μM, 0.055 μM, 0.351 μM and 0.025 μM, respectively.[108] An integrated microfluidic-based electrochemical sensor was fabricated by Dai *et al.* for Pb^{2+} detection. The sensor was made up of three layers, and the RE was fabricated on the first layer. The third layer was integrated with a Au micropillar array (3D) WE and a planar Au CE on a glass substrate. This three-layered sensor, composed of glass–silicon–glass, was formed through the bonding of two electrode layers and a silicon layer. The quantification of Pb^{2+} was achieved by SWASV. The Cd^{2+}, Cu^{2+}, and Hg^{2+} heavy metals were found to cause interference in the detection of Pb^{2+}, which can be minimized in the presence of the masking agents. The LOD was found to be 0.13 ppb.[118] A screen-printed electrode was fabricated by Bernalte *et al.* for the simultaneous detection of heavy metals such as Cu, Pb^{2+}, and Hg^{2+}. The WE, RE, and CE were fabricated using gold ink and silver ink, respectively. Using SWASV, the heavy metals were quantified. The LODs of Cu^{2+}, Pb^{2+} and Hg were found to be 1.3 mg L^{-1}, 0.015 mg L^{-1} and 0.002 mg L^{-1}, respectively.[114] The modification of the WE with various materials will increase the sensitivity of the electrochemical sensor toward detecting specific heavy metals.[97] For example, multiwalled carbon nanotube–PANI nanocomposites were used in the surface modification of glassy carbon electrodes for Pb^{2+} detection.[119] The electrodes were modified with AuNPs and AgNPs to improve the LOD. A paper-based electrochemical device was developed by Pungjunun *et al.*, where a boron-doped diamond electrode modified with AuNPs (AuNP/BDD) was used in As^{3+} detection. Screen-printed carbon and Ag/AgCl were used as the CE and RE, respectively. Interference from Cu^{2+} was detected in the procedure but was successfully eliminated using ferricyanide. The LOD was determined to be 20 ng mL^{-1}.[120]

Conclusion

This review has highlighted the role of devices using microfluidics to detect heavy metals. The field of microfluidic-based heavy metal detection is rapidly advancing and finding applications not only in environmental monitoring but also in other fields of research, such as food technology and health care. These devices are being developed to compensate for existing complex and expensive procedures. The development of real-time devices, that can provide quick results and can be operated without experienced people, has become a new trend in the field of microfluidics. Most of the developed devices are believed to have the same sensitivity and accuracy as the current detection methods. In this review, we have discussed various techniques used in detecting different heavy metals, such as colorimetry, absorbance-based techniques, and electrochemical detection. The *in situ* and real-time monitoring of these techniques is crucial for the identification and mitigation of heavy metal contamination. Microfluidic technologies will continue to advance, offering great sensitivity, selectivity, and portability. However, there are few shortcomings which need to be addressed. Most of the existing microfluidics devices focus on the detection of single heavy metals; simultaneous detection remains a challenge. This can be improved by integrating multiple detection techniques such as colorimetry, absorbance-based detection and electrochemical detection in a single device that in turn improves the sensitivity. A prominent challenge in analysis is that the LOD can differ across different heavy metal samples and can be improved by optimization of the device and improving the surface chemistry of the sensors. Even though microfluidic-based devices are portable and used in real time detection, data interpretation and analysis are time consuming. The integration of artificial intelligence (AI) and machine learning (ML) in detection not only improves the data analysis, but it can also reduce the interference from other elements present in the real samples.

Author contributions

N. M. created the outline of this review. S. S. N. wrote the manuscript and designed the figures. N. M. and R. B. reviewed and edited the manuscript.

Conflicts of interest

The authors do not have any conflict of interest.

Acknowledgements

NM thanks the Department of Science and Technology (DST) (Project Number – SERB/MTR/2020/000058) and the Indian Council of Medical Research (ICMR) (Project Number – ITR/Ad hoc/43/2020-21, ID No. 2020-3286) Government of India, India, for financial support. RB thanks the Biotechnology Industry Research Assistance Council (BIRAC), Department of Biotechnology, Government of India, India (Proposal number: BIRAC/KIIT01165/BIG-17/20), for financial support. NM and SSN thank the Manipal School of Life Sciences, Manipal Academy of Higher Education (MAHE), Manipal, Karnataka, India, for providing the infrastructure. SSN thanks MAHE, Manipal, Karnataka, India for the Dr T. M. A. Pai PhD fellowship.

References

1 S. H. A. Koop and C. J. van Leeuwen, *Environ. Dev. Sustain.*, 2017, **19**, 385–418.

2 P. Lentini, L. Zanoli, A. Granata, S. S. Signorelli, P. Castellino and R. Dellaquila, *Mol. Med. Rep.*, 2017, **15**, 3413–3419.
3 M. Balali-Mood, K. Naseri, Z. Tahergorabi, M. R. Khazdair and M. Sadeghi, *Front. Pharmacol*, 2021, **12**, 643972.
4 A. Bahrami, M. R. Arabestani, M. Taheri, A. Farmany, F. Norozzadeh, S. M. Hosseini, H. Nozari and F. Nouri, *Biol. Trace Elem. Res.*, 2022, **200**, 2639–2650.
5 J. Hogervorst, M. Plusquin, J. Vangronsveld, T. Nawrot, A. Cuypers, E. Van Hecke, H. A. Roels, R. Carleer and J. A. Staessen, *Environ. Res.*, 2007, **103**, 30–37.
6 S. Mishra, R. N. Bharagava, N. More, A. Yadav, S. Zainith, S. Mani and P. Chowdhary, in *Springer eBooks*, 2018, pp. 103–125.
7 E. G. C. Clarke, *J. Small Anim. Pract.*, 1973, **14**, 183–194.
8 W. R. Cullen and K. J. Reimer, *Chem. Rev.*, 1989, **89**, 713–764.
9 E. Diesel, M. Schreiber and J. R. van der Meer, *Anal. Bioanal. Chem.*, 2009, **394**, 687–693.
10 A. G.-M. Ferrari, P. Carrington, S. J. Rowley-Neale and C. E. Banks, *Environ. Sci.*, 2020, **6**, 2676–2690.
11 G. Matta and L. Gjyli, *J. Chem. Pharm. Sci.*, 2016, **9**, 718–725.
12 P. B. Tchounwou, W. K. Ayensu, N. Ninashvili and D. Sutton, *Environ. Toxicol.*, 2003, **18**, 149–175.
13 K. Eto, *Neuropathology*, 2000, **20**, 14–19.
14 G. S. Dheri, M. S. Brar and S. S. Malhi, *Commun. Soil Sci. Plant Anal.*, 2007, **38**, 1353–1370.
15 A. Thongsaw, R. Sananmuang, Y. Udnan, R. J. Ampiah-Bonney and W. C. Chaiyasith, *Anal. Sci.*, 2019, **35**, 1195–1202.
16 H. Zheng, J. Hong, X. Luo, S. Li, M. Wang, B. Yang and M. Wang, *Microchem. J.*, 2019, **145**, 806–812.
17 T. Narukawa, T. Iwai and K. Chiba, *Talanta*, 2020, **210**, 120646.
18 H. K. Sunaina, N. Kumari, A. Sharma, M. Sachdeva and V. Mutreja, *Mater. Today: Proc.*, 2022, **48**, 1673–1679.
19 L.-L. Shen, G.-R. Zhang, W. Li, M. Biesalski and B. J. M. Etzold, *ACS Omega*, 2017, **2**, 4593–4603.
20 J. Hwang, Y. H. Cho, M. S. Park and B. H. Kim, *Int. J. Precis. Eng. Manuf.*, 2019, **20**, 479–495.
21 G. Aragay and A. Merkoçi, *Electrochim. Acta*, 2012, **84**, 49–61.
22 Y. F. Wisang, H. Sulistyarti, U. Andayani and A. Sabarudin, *IOP Conf. Ser.: Mater. Sci. Eng.*, 2019, **546**, 032033.
23 A. Lace and J. Cleary, *Chemosensors*, 2021, **9**, 60.
24 M. K. Filippidou, A. I. Kanaris, E. Aslanidis, A. Rapesi, D. Tsounidi, S. Ntouskas, E. Skotadis, G. Tsekenis, D. Tsoukalas, A. Tserepi and S. Chatzandroulis, *Micromachines*, 2023, **14**, 1595.
25 G. Chen, X. Wang and L. Wang, *Int. J. Electrochem. Sci.*, 2020, **15**, 4252–4263.
26 D. Janasek, J. Franzke and A. Manz, *Nature*, 2006, **442**, 374–380.
27 D.-E. Li and C.-H. Lin, *RSC Adv.*, 2018, **8**, 16139–16145.
28 D. Wu, S. Yang, F. Li, T. Zhu and H. Chen, *Anal. Chem.*, 2020, **92**, 14309–14313.
29 B.-H. Chen, S.-J. Jiang and A. C. Sahayam, *Food Chem.*, 2020, **324**, 126698.
30 N. Burshtein, S. T. Chan, K. Toda-Peters, A. Q. Shen and S. J. Haward, *Curr. Opin. Colloid Interface Sci.*, 2019, **43**, 1–14.
31 H. Wang, H. Rao, M. Luo, X. Xue, X. Zhang and X. Lu, *Coord. Chem. Rev.*, 2019, **398**, 113003.
32 F. Zhu, Y. He, Z. Lu, H. Fan and T. Zhang, *ACS Appl. Mater. Interfaces*, 2021, **13**, 37589–37597.
33 A. H. McMillan, M. Roeffaers and S. C. Lesher-Pérez, *Thermoplastic elastomer microfluidic devices for biology and chemistry*, University of Vienna, 2021.
34 E. L. Fava, T. A. Silva, T. M. do Prado, F. C. de Moraes, R. C. Faria and O. Fatibello-Filho, *Talanta*, 2019, **203**, 280–286.
35 S. C. Terry, J. H. Jerman and J. B. Angell, *IEEE Trans. Electron Devices*, 1979, **26**, 1880–1886.
36 W. H. Grover, R. H. C. Ivester, E. C. Jensen and R. A. Mathies, *Lab Chip*, 2006, **6**, 623.
37 P. N. Nge, C. I. Rogers and A. T. Woolley, *Chem. Rev.*, 2013, **113**, 2550–2583.
38 S. Aralekallu, R. Boddula and V. Singh, *Mater. Des.*, 2023, **225**, 111517.
39 S. Funano, N. Ota and Y. Tanaka, *Lab Chip*, 2021, **21**, 2244–2254.
40 K. Ren, J. Zhou and H. Wu, *Acc. Chem. Res.*, 2013, **46**, 2396–2406.
41 J. C. McDonald, D. C. Duffy, J. R. Anderson, D. T. Chiu, H. Wu, O. J. A. Schueller and G. M. Whitesides, *Electrophoresis*, 2000, **21**, 27–40.
42 H. Wu, T. W. Odom, D. T. Chiu and G. M. Whitesides, *J. Am. Chem. Soc.*, 2003, **125**, 554–559.
43 J. Shim, G. Cristobal, D. R. Link, T. Thorsen, Y. Jia, K. Piattelli and S. Fraden, *J. Am. Chem. Soc.*, 2007, **129**, 8825–8835.
44 G. T. Roman, T. Hlaus, K. J. Bass, T. G. Seelhammer and C. T. Culbertson, *Anal. Chem.*, 2005, **77**, 1414–1422.
45 H. Becker and C. Gärtner, *Anal. Bioanal. Chem.*, 2008, **390**, 89–111.
46 C.-W. Tsao and D. L. DeVoe, *Microfluid. Nanofluid.*, 2009, **6**, 1–16.
47 A. W. Martinez, S. T. Phillips, M. J. Butte and G. M. Whitesides, *Angew. Chem.*, 2007, **119**, 1340–1342.
48 S. A. Klasner, A. K. Price, K. W. Hoeman, R. S. Wilson, K. J. Bell and C. T. Culbertson, *Anal. Bioanal. Chem.*, 2010, **397**, 1821–1829.
49 D. Wu, S. Yang, F. Li, T. Zhu and H. Chen, *Anal. Chem.*, 2020, **92**, 14309–14313.
50 W. Cui, Z. Ren, Y. Song and C. L. Ren, *Sens. Actuators, A*, 2022, **344**, 113733.
51 S. B. D. Borah, T. Bora, S. Baruah and J. Dutta, *Groundw. Sustain. Dev.*, 2015, **1**, 1–11.
52 W. M. E. M. M. Daniyal, Y. W. Fen, N. I. M. Fauzi, H. S. Hashim, N. S. M. Ramdzan and N. A. S. Omar, *Sens. Mater.*, 2020, **32**, 4191.
53 P. Aryal, E. Brack, T. Alexander and C. S. Henry, *Anal. Chem.*, 2023, **95**, 5820–5827.
54 J. P. Devadhasan and J. Kim, *Sens. Actuators, B*, 2018, **273**, 18–24.

55 H. Wang, H. Rao, M. Luo, X. Xue, Z. Xue and X. Lu, *Coord. Chem. Rev.*, 2019, **398**, 113003.
56 M. J. Kangas, R. M. Burks, J. Atwater, R. M. Lukowicz, P. Williams and A. E. Holmes, *Crit. Rev. Anal. Chem.*, 2017, **47**, 138–153.
57 M. L. Budlayan, J. Dalagan, J. P. Lagare-Oracion, J. Patricio, S. Arco, F. Latayada, T. Vales, B. Baje, A. Alguno and R. Capangpangan, *Environ. Nanotechnol., Monit. Manage.*, 2022, **18**, 100736.
58 B. Sahu, R. Kurrey, M. K. Deb, K. Shrivas, I. Karbhal and B. R. Khalkho, *RSC Adv.*, 2021, **11**, 20769–20780.
59 P. Yeh, N. Yeh, C.-H. Lee and T.-J. Ding, *Renewable Sustainable Energy Rev.*, 2017, **75**, 461–468.
60 S. A. A. Razavi and A. Morsali, *Coord. Chem. Rev.*, 2020, **415**, 213299.
61 A. Lace, D. Ryan, M. Bowkett and J. Cleary, *Anal. Methods*, 2019, **11**, 5431–5438.
62 B. Karakuzu, Y. Gulmez and H. C. Tekin, *Microelectron. Eng.*, 2021, **247**, 111583.
63 X. Xie, M. Pan, L. Hong, K. Liu, J. Yang, S. Wang and S. Wang, *J. Agric. Food Chem.*, 2021, **69**, 7209–7217.
64 Y. C. Reyes R, T. B. Rouf, O. E. Torres and E. E. González, *ACS Agric. Sci. Technol.*, 2022, **2**, 144–152.
65 S. Singh, B. Coulomb, J.-L. Boudenne, D. Bonne, F. Dumur, B. Simon and F. Robert-Peillard, *Talanta*, 2021, **224**, 121909.
66 K. Karthikeyan and L. Sujatha, *IEEE Sens. J.*, 2018, **18**, 5225–5231.
67 G. Peng, Y. Chen, R. Deng, Q. He, D. Liu, Y. Lu and J.-M. Lin, *Spectrochim. Acta, Part A*, 2018, **204**, 1–6.
68 H. Yuan, G. Sun, W. Peng, W. Ji, S. Chu, Q. Liu and Y. Liang, *Nanomaterials*, 2021, **11**, 397.
69 W. Huang, V. Phung, R.-Y. Wu, K.-L. Yeh and R.-J. Yang, *Micromachines*, 2021, **12**, 1283.
70 A. Biranje, N. Azmi, A. Tiwari and A. Chaskar, *J. Fluoresc.*, 2021, **31**, 1241–1250.
71 J. Yue, Q. Lv, W. Wang and Q. Zhang, *Talanta Open*, 2022, **5**, 100099.
72 J. Qi, B. Li, X. Wang, Z. Zhang, Z. Wang, J. Han and L. Chen, *Sens. Actuators, B*, 2017, **251**, 224–233.
73 L. Wang, B. Li, J. Wang, J. Qi, J. Li, J. Ma and L. Chen, *J. Hazard. Mater.*, 2022, **428**, 128165.
74 L. Wang, B. Li, J. Li, J. Qi, Z. Zhang and L. Chen, *Analyst*, 2022, **147**, 3756–3763.
75 J. Han, H. Liu, J. Qi, J. Xiang, L. Fu, X. Sun, L. Wang, X. Wang, B. Li and L. Chen, *Sensors*, 2023, **23**, 3094.
76 J. Zhou, B. Li, A. Qi, Y. Shi, J. Qi, H. Xu and L. Chen, *Sens. Actuators, B*, 2020, **305**, 127462.
77 X. Wang, L. Kong, Y. Gan, T. Liang, S. Zhou, J. Sun, H. Wan and P. Wang, *Anal. Chim. Acta*, 2020, **1131**, 126–135.
78 M. Lu, Y. Deng, Y. Luo, J. Lv, T. Li, J. Xu, S.-W. Chen and J. Wang, *Anal. Chem.*, 2019, **91**, 888–895.
79 R. M. El-Shishtawy, H. A. Al-Ghamdi, M. M. Alam, Z. M. Al-amshany, A. M. Asiri and M. M. Rahman, *Chem. Eng. J.*, 2018, **352**, 225–231.
80 N. Wongkaew, P. He, V. Kurth, W. Surareungchai and A. J. Baeumner, *Anal. Bioanal. Chem.*, 2013, **405**, 5965–5974.
81 H. Hou, K. M. Zeinu, S. Gao, B. Liu, J. Yang and J. Hu, *Energy Environ. Mater.*, 2018, **1**, 113–131.
82 T. D. Nguyen, M. T. N. Nguyen and J. S. Lee, *Inorganics*, 2023, **11**, 81.
83 S. Liu, T. Wu, F. Li, Q. Zhang, X. Dong and L. Niu, *Anal. Methods*, 2018, **10**, 1986–1992.
84 J.-H. Hwang, X. Wang, D. Zhao, M. M. Rex, H. J. Cho and W. H. Lee, *Electrochim. Acta*, 2019, **298**, 440–448.
85 P. B. Deroco, D. Wachholz Junior and L. T. Kubota, *Chemosensors*, 2021, **9**, 61.
86 F. Wang, S. Wang, L. Zhang, H. Yang, W. Gao, Q. Wu and J. Hao, *J. Environ. Sci.*, 2016, **43**, 293–301.
87 W. Zhang, G. Liu, J. Bi, K. Bao and P. Wang, *Sens. Actuators, A*, 2023, **349**, 114074.
88 Y. Li, F. Ye, A. Wang, D. Wang, B. Yang, Q. Zheng, G. Sun and X. Gao, *Int. J. Environ. Res. Public Health*, 2016, **13**, 133.
89 R. A. G. de Oliveira, E. M. Materon, M. E. Melendez, A. L. Carvalho and R. C. Faria, *ACS Appl. Mater. Interfaces*, 2017, **9**, 27433–27440.
90 S. Singh, J. Wang and S. Cinti, *ECS Sens. Plus*, 2022, **1**, 023401.
91 N. Zavanelli and W.-H. Yeo, *ACS Omega*, 2021, **6**, 9344–9351.
92 H. Shamkhalichenar and J.-W. Choi, *ECS Meeting Abstracts*, 2017, MA2017-01, p. 1879.
93 K. Zub, S. Hoeppener and U. S. Schubert, *Adv. Mater.*, 2022, **34**, 2105015.
94 S. Diaz-Amaya, L.-K. Lin, R. E. DiNino, C. Ostos and L. A. Stanciu, *Electrochim. Acta*, 2019, **316**, 33–42.
95 A. Ambrosi and M. Pumera, *Chem. Soc. Rev.*, 2016, **45**, 2740–2755.
96 R. M. Cardoso, C. Kalinke, R. G. Rocha, P. L. dos Santos, D. P. Rocha, P. R. Oliveira, B. C. Janegitz, J. A. Bonacin, E. M. Richter and R. A. A. Munoz, *Anal. Chim. Acta*, 2020, **1118**, 73–91.
97 B. Bansod, T. Kumar, R. Thakur, S. Rana and I. Singh, *Biosens. Bioelectron.*, 2017, **94**, 443–455.
98 G. Lisak, *Environ. Pollut.*, 2021, **289**, 117882.
99 S. Chauhan and L. S. B. Upadhyay, *J. Ravishankar Univ., Part B*, 2019, **32**, 23–26.
100 G. Le Guillanton, Q. T. Do and D. Elothmani, *J. Electrochem. Soc.*, 1996, **143**, L223–L225.
101 J. Zhou, K. Ren, Y. Zheng, J. Su, Y. Zhao, D. Ryan and H. Wu, *Electrophoresis*, 2010, **31**, 3083–3089.
102 G.-L. Wen, W. Zhao, X. Chen, J.-Q. Liu, Y. Wang, Y. Zhang, Z.-J. Huang and Y.-C. Wu, *Electrochim. Acta*, 2018, **291**, 95–102.
103 H. A. Hamid, Z. Lockman, N. M. Nor, N. D. Zakaria and K. A. Razak, *Mater. Chem. Phys.*, 2021, **273**, 125148.
104 H. Men, S. Zou, Y. Li, Y. Wang, X. Ye and P. Wang, *Sens. Actuators, B*, 2005, **110**, 350–357.
105 B. S. Sherigara, Y. Shivaraj, R. J. Mascarenhas and A. K. Satpati, *Electrochim. Acta*, 2007, **52**, 3137–3142.
106 W. Jung, A. Jang, P. L. Bishop and C. H. Ahn, *Sens. Actuators, B*, 2011, **155**, 145–153.
107 D. B. Sheth and M. Gratzl, *Anal. Bioanal. Chem.*, 2013, **405**, 5539–5547.

108 Z. Xu, Z. Liu, M. Xiao, L. Jiang and C. Yi, *Chem. Eng. J.*, 2020, **394**, 124966.
109 G. Luka, A. Ahmadi, H. Najjaran, E. Alocilja, M. DeRosa, K. Wolthers, A. Malki, H. Aziz, A. Althani and M. Hoorfar, *Sensors*, 2015, **15**, 30011–30031.
110 Y. Hong, M. Wu, G. Chen, Z. Dai, Y. Zhang, G. Chen and X. Dong, *ACS Appl. Mater. Interfaces*, 2016, **8**, 32940–32947.
111 A. M. Baracu and L. A. Dinu Gugoasa, *J. Electrochem. Soc.*, 2021, **168**, 037503.
112 H.-F. Li and J.-M. Lin, *Anal. Bioanal. Chem.*, 2009, **393**, 555–567.
113 C. Kokkinos, A. Economou and D. Giokas, *Sens. Actuators, B*, 2018, **260**, 223–226.
114 E. Bernalte, S. Arévalo, J. Pérez-Taborda, J. Wenk, P. Estrela, A. Avila and M. Di Lorenzo, *Sens. Actuators, B*, 2020, **307**, 127620.
115 J. M. Mohan, S. Dudala, K. Amreen, A. Javed, S. K. Dubey and S. Goel, *IEEE Trans. NanoBiosci.*, 2023, **22**, 881–888.
116 M. F. Santangelo, I. Shtepliuk, D. Filippini, D. Puglisi, M. Vagin, R. Yakimova and J. Eriksson, *Sensors*, 2019, **19**, 2393.
117 V. Subramanian, S. Lee, S. Jena, S. K. Jana, D. Ray, S. J. Kim and P. Thalappil, *Sens. Actuators, B*, 2020, **304**, 127340.
118 J. Dai, W. Gao, J. Yin, L. Liang, J. Zou and Q. Jin, *Anal. Chim. Acta*, 2021, **1164**, 338511.
119 Z. Wang, E. Liu, D. Gu and Y. Wang, *Thin Solid Films*, 2011, **519**, 5280–5284.
120 K. Pungjunun, S. Chaiyo, I. Jantrahong, S. Nantaphol, W. Siangproh and O. Chailapakul, *Microchim. Acta*, 2018, **185**, 324.
121 R. A. Schwartz, *Int. J. Dermatol.*, 1997, **36**, 241–250.
122 H. Garelick, H. Jones, A. Dybowska and E. Valsami-Jones, *Rev. Environ. Contam. Toxicol.*, 2009, 17–60.
123 L. Joseph, B.-M. Jun, J. R. V. Flora, C. M. Park and Y. Yoon, *Chemosphere*, 2019, **229**, 142–159.
124 D. L. Alonso, R. Pérez, C. K. Y. A. Okio and E. Castillo, *J. Environ. Manage.*, 2020, **264**, 110478.
125 W. Ramos, A. G. Ortega-Loayza, J. Díaz, J. A. De La Cruz-Vargas, M. Tello, G. Ronceros, M. Loayza and E. L. Gutierrez, *Clin., Cosmet. Invest. Dermatol.*, 2022, **15**, 2407–2414.
126 T. C. Nguyen, P. Loganathan, T. V. Nguyen, S. Vigneswaran, J. Kandasamy and R. Naidu, *Chem. Eng. J.*, 2015, **270**, 393–404.
127 M. Mezynska and M. M. Brzóska, *Environ. Sci. Pollut. Res.*, 2018, **25**, 3211–3232.
128 T. Umemura and Y. Wako, *J. Toxicol. Pathol.*, 2006, **19**, 69–74.
129 L. Järup, *Nephrol., Dial., Transplant.*, 2002, **17**, 35–39.
130 L. Patrick, *Alternative Med. Rev.*, 2003, **8**, 106–128.
131 C. J. Everett and I. L. Frithsen, *Environ. Res.*, 2008, **106**, 284–286.
132 P. B. Tchounwou, W. K. Ayensu, N. Ninashvili and D. Sutton, *Environ. Toxicol.*, 2003, **18**, 149–175.
133 B. Tripathy, A. Dash and A. P. Das, *Crit. Rev. Anal. Chem.*, 2022, 1–11.
134 I. Manisalidis, E. Stavropoulou, A. Stavropoulos and E. Bezirtzoglou, *Front. Public Health*, 2020, **8**, 505570.
135 E. G. C. Clarke, *J. Small Anim. Pract.*, 1973, **14**, 183–194.
136 A. L. Wani, A. Ara and J. A. Usmani, *Interdiscip. Toxicol.*, 2015, **8**, 55–64.
137 K. Raj and A. P. Das, *Environ. Chem. Ecotoxicol.*, 2023, **5**, 79–85.
138 Z. Rahman and V. P. Singh, *Environ. Monit. Assess.*, 2019, **191**, 419.
139 C. Lidén, *Br. J. Dermatol.*, 2013, **169**, 733.
140 Q. Y. Chen, J. Brocato, F. Laulicht and M. Costa, in *Molecular and Integrative Toxicology*, 2017, vol. 8, pp. 181–197.
141 W. Dong, Y. Zhang and X. Quan, *Chemosphere*, 2020, **242**, 125113.
142 S. Albanese, M. Sadeghi, A. Lima, D. Cicchella, E. Dinelli, P. Valera, M. Falconi, A. Demetriades and B. De Vivo, *J. Geochem. Explor.*, 2015, **154**, 81–93.
143 M. Babaahmadifooladi, L. Jacxsens, B. De Meulenaer and G. Du Laing, *Food Addit. Contam.: Part A*, 2020, **37**, 607–621.
144 L. Leyssens, B. Vinck, C. Van Der Straeten, F. Wuyts and L. Maes, *Toxicology*, 2017, **387**, 43–56.
145 W. Uter, R. Rühl, A. Pfahlberg, J. Geier, A. Schnuch and O. Gefeller, *Ann. Occup. Hyg.*, 2004, **48**, 21–27.
146 P. N. Bezerra, A. G. A. Vasconcelos, L. L. A. Cavalcante, V. B. d. V. Marques, T. N. A. G. Nogueira and M. A. Holanda, *J. Bras. Pneumol.*, 2009, **35**, 1254–1258.
147 B. Zhao, M. He, B. Chen and B. Hu, *Spectrochim. Acta, Part B*, 2022, **196**, 106524.
148 M. Ghanei-Motlagh and M. Baghayeri, *Mater. Chem. Phys.*, 2022, **285**, 126127.
149 Y. Xing, J. Han, X. Wu, D. T. Pierce and J. X. Zhao, *Microchim. Acta*, 2020, **187**, 56.
150 D. Mishra, A. Krause, H. S. Sahni and S. Chatterjee, *Diamond Relat. Mater.*, 2023, **137**, 110156.
151 G. Vyas, S. Bhatt and P. Paul, *ACS Omega*, 2019, **4**, 3860–3870.
152 H. R. Cadorim, M. Schneider, J. Hinz, F. Luvizon, A. N. Dias, E. Carasek and B. Welz, *Anal. Lett.*, 2019, **52**, 2133–2149.
153 A. Bhat, T. O. Hara, F. Tian and B. Singh, *Environ. Sci.: Adv.*, 2023, **2**, 171–195.
154 T. Agustiany, M. Khalil, Y. Einaga, P. K. Jiwanti and T. A. Ivandini, *Mater. Chem. Phys.*, 2020, **244**, 122723.
155 C. G. A. Maria, A. S. Agnihotri, A. Varghese, T. Fatima and S. Hameed, *New J. Chem.*, 2023, **47**, 5179–5192.
156 J. You, J. Li, Z. Wang, M. Baghayeri and H. Zhang, *Chemosphere*, 2023, **335**, 139133.
157 J. Zhou, D. Deng, Y. Su and Y. Lv, *Microchem. J.*, 2019, **146**, 359–365.
158 P. Montoro-Leal, J. C. García-Mesa, M. T. Siles Cordero, M. M. López Guerrero and E. Vereda Alonso, *Microchem. J.*, 2020, **155**, 104796.
159 S. Chen, J. Yan, J. Li and D. Lu, *Microchem. J.*, 2019, **147**, 232–238.
160 L. A. Malik, A. Bashir, A. Qureashi and A. H. Pandith, *Environ. Chem. Lett.*, 2019, **17**, 1495–1521.

161 Y. A. Ghorbani, S. M. Ghoreishi and M. Ghani, *Microchem. J.*, 2020, **155**, 104786.
162 S. Sel, F. A. Erulaş, F. Turak and S. Bakırdere, *Anal. Lett.*, 2019, **52**, 761–771.
163 A. Karthika, S. Nikhil, A. Suganthi and M. Rajarajan, *Adv. Powder Technol.*, 2020, **31**, 1879–1890.
164 H. Sharifi, J. Tashkhourian and B. Hemmateenejad, *Anal. Chim. Acta*, 2020, **1126**, 114–123.
165 P. Kamnoet, W. Aeungmaitrepirom, R. F. Menger and C. S. Henry, *Analyst*, 2021, **146**, 2229–2239.
166 H. Taheri and G. Khayatian, *Spectrochim. Acta, Part A*, 2022, **272**, 121000.
167 X. Sun, B. Li, A. Qi, C. Tian, J. Han, Y. Shi, B. Lin and L. Chen, *Talanta*, 2018, **178**, 426–431.